JP&M Engineering
Journal of Petroleum and Mining Engineering
http://jpme.journals.ekb.eg/

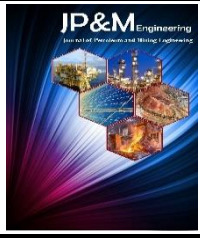

Synthesis and Evaluation of Strengthened Copper with 3 wt. % TiC and/ or Al_2O_3 Prepared by SPS Technique

Hamed, F. S.,[a*] Elsayed, A.[b], Elkady, O.[b] , EL-Nikhaily, A [a], and Essa, A.[a,c]
[a] Mechanical Production Department, Faculty of Technology and education, Suez University
[b] Central Metallurgical Research and Development Institute, Egypt
[c] Egyptian Academy for Engineering & Advanced Technology, Affiliated to Ministry of Military Production, Egypt
*Corresponding author e-mail: fadel.shaban@suezuni.edu.eg

Article Info

Received 21 Mar. 2021
Revised 3 May 2021
Accepted 23 May 2021

Keywords

Copper composite; Nano TiC; Nano Al_2O_3; Hybrid reinforcement; Microstructure; Tribological properties; Electrical conductivity; Thermal conductivity.

Abstract

Cu-(TiC/Al_2O_3) nanocomposite was synthesized successfully using the powder metallurgy route. The constituents are first ball-milled and then sintered using the spark plasma sintering technique. The tribological and physical properties are investigated. The homogeneity and of ceramics distribution were also evaluated using SEM and XRD. Results showed that TiC and Al_2O_3 nanoparticles were homogeneously distributed all over the Cu matrix. Copper reinforced with 3 wt.% Al_2O_3 and hybrid (3 wt.% TiC and Al_2O_3) had the lowest relative density (95%). The hybrid (3wt. % TiC and Al_2O_3) sample had a higher wear rate value ($1.7*10^{-3}$) at 25 N load, while the sample reinforced with 3 wt.% TiC had the lowest value ($0.5*10^{-3}$) at 25 N load. Cu-Al_2O_3 exhibited a higher hardness value (149 HV). The highest electrical and thermal conductivities are recorded for the Cu-TiC that were (20.76 MS/m) and (149.03 W/m. k) respectively

Introduction

Copper (Cu) has a low substantial strength, poor mechanical properties, and a high coefficient of thermal expansion. It is well recognized that the addition of hard ceramic materials to pure copper can meaningfully improve the mechanical properties and wear resistance, titanium carbide (TiC) and alumina (Al_2O_3) nanoparticles are typical reinforcement phases [1][2], due to high wear resistance, high strength and stiffness, high melting point and superior mechanical properties at high temperature and low cost [3] [4]. The incorporation of fine TiC and Al_2O_3 particles in the copper matrix improves the hardness and decreases the rate of grain growth at high temperatures [5].

High-Pressure Spark Plasma Sintering (HSPS) is a unique technique for the preparation of many materials of poor sinter capability, for example, ceramic composites, super hard materials, or refractory materials based on boron nitride or polycrystalline diamond. It is also possible to sinter materials based on intermetallic alloys [6][7]. High-Pressure Spark Plasma Sintering is a unique new option of well-established Spark Plasma Sintering alumina, titanium carbide, zirconium diboride [8], silicon carbide ceramics [9], and molybdenum disilicate [10], were prepared using this device.

Ultra-high pressure (up to 8 GPa) and quick times of sintering are characterized in this technique. The objective of sintering at high pressure is to protect the fine grain structure of the material, simplify a new grain arrangement, limit recrystallization processes activated by increased temperature during sintering, decrease diffusion during the sintering, and obtain non-porous solid material [10][11]. A high pulsed direct current flows through the powder material, which activates the sintering reaction. Micro-spark discharges occur in the spaces between powder particles, and plasma is generated [12]. These discharges remove absorbed gases and oxide films on powder particles [12]. The surface of the particles is activated by heat and strain energy. A power source generates Joule heating in places with activated particles and causes thermal electron diffusion. Micro-spark discharges together with the ultra-high pressure cause perfect sintering of the material [13].

There are several ceramic reinforcements, such as SiC [20], TiC [21], Al_2O_3 [22], ZrO_2 [23], GO [24], La_2O_3 [25], ZrB_2 [26], CNTs [27], CNTs-Gr hybrid [28], TiC-SiC hybrid [29], have been used to boost the mechanical properties of Cu, usually at the expense of electrical and thermal conductivity. The incorporation of chemically stable hard ceramic particles is an alternative and feasible method for improving the mechanical and wear action of Cu. Among the available reinforcements, titanium carbide (TiC) and alumina (Al_2O_3) have high hardness (2850-3550 HV) and (1937-2141 HV), respectively, and can increase the abrasion resistance of many alloy systems [12][30]. Because of their high hardness, stiffness, chemical stability, and excellent wear resistance, TiC and Al_2O_3 are commonly used in the production of metallic friction

composites. They have been shown to play critical roles in strengthening composites and optimizing tribological efficiency [31][32].

The interest in dual and hybrid reinforcements is growing because some individual reinforcements are still incapable of imparting the desired properties. For example, the inverse relationship between strength and ductility has put researchers in a dilemma as both properties appear to conflict with each other [13,29]. Hence, some researchers incorporated an additional element, so that the additional reinforcement would provide what is lacking in main reinforcement [36]. In the present work, pure copper reinforced with nano TiC or Al_2O_3 nano particulates, and their effects on the mechanical properties are investigated. Reinforcements are dispersed in the copper matrix via low energy ball milling, and the admixed powders are consolidated by HSPS [37]. Hybrid sintering is a recently developed technique used in materials fabrication, which provides superior heating within and across the material regime. It integrates the heating system of spark plasma sintering with an additional resistance or induction heating to manufacture materials that require a larger size or diameter. Materials prepared by this technique are highly dense due to the rapid heating rate which ensues in a very short sintering cycle. Hybrid sintering eliminates the thermal gradient that is noticeable in other sintering techniques. Fabricated materials from HSPS are utilized in aerospace, automobile, and chemical industries and improved mechanical properties [37].

In the present work, Cu–TiC, Cu–Al_2O_3 composites, and Cu–TiC/Al_2O_3 hybrid nanocomposites were prepared by spark plasma sintering (SPS) to investigate the effect of TiC and Al_2O_3 nanoparticles content on microstructure, physical, and tribological properties. Another possibility to achieve a better mechanical performance of Cu–TiC and Cu-Al_2O_3 is the use of copper powders with a smaller percentage particle size.

Materials and Methods

Materials

Copper powder with 99.9% purity (supplied by Alpha Chemicals, USA) and 50µm particle size is used as a metal matrix. Alumina powder with 99.7% purity (supplied by Alpha Chemicals, USA) with an average particle size of 50 nm is used as a reinforcement material. Titanium carbide powder with 99.7% purity (supplied by Inframat Advanced Materials, LLC, Manchester, USA) with 100 nm average particle size is used as another reinforcement. Four samples are prepared, the Cu pure, 3wt.% TiC, 3wt. % Al_2O_3, and hybrid from 3wt.% TiC and Al_2O_3 (fifty-fifty) are mixed using a ball mill technique for 24 hr. The powders are mixed by 25:1 ball to powder ratio (BPR), 110 rpm and a ball diameter of 5 mm under atmosphere pure argon gas to be protected from any oxidation, Stearic acid (1.5 wt.%) is used as a process controlling agent (PCA). A mixing process was carried out in the Faculty of Technology and Education, Suez University. Table-1 and Fig.1 show the composition and nomenclature of prepared specimens.

SPARK PLASMA SINTERING

Sintering experiments are performed using spark plasma sintering (DR. SINTER LAB Model: SPS-1030, SPS Syntex,

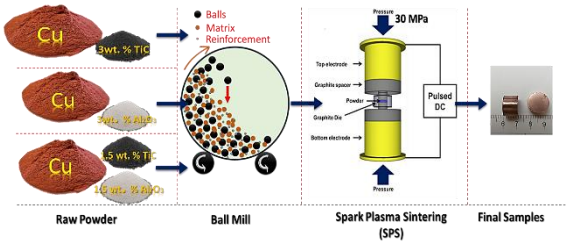

Figure 1 Schematic diagram of Cu with TiC and Al2O3 and hybrid nano reinforcement composites.

Table 1 Composition and nomenclature of prepared specimens

No	Sample Code	Composition		
		Matrix	Reinforcement	
		Cu	TiC	Al_2O_3
1	S00	100 wt. %	0 wt. %	0 wt. %
2	S01	97 wt. %	3 wt. %	0 wt. %
3	S02	97 wt. %	0 wt. %	3 wt. %
4	S03	97 wt. %	1.5 wt. %	1.5 wt. %

Japan). The powder is loaded into a graphite die with 15 mm diameter with graphite foil and enclitic by 0.5 mm thick graphite cover to minimize heat desperation. Before sintering, the SPS chamber is pumped to a pressure below 5 Pa. The samples are heated from room temperature up to 950˚C by pulsed DC current passing through the graphite die, punches, and the sample itself. Samples are held at maximum temperature for 45 min, the heating rate is 20˚C/min at a uniaxial pressure of 30 Mpa. Spark plasma sintering (SPS) was carried out in the Composite Materials Processing lab., JWRI, Osaka University. Shows a schematic diagram for the PM preparation method for Cu-TiC / Al_2O_3 composites, Fig.1.

Composite Characterization

The density of copper composite is determined according to Archimedes' principle as per ASTM B311-93 [38]. It is estimated by measuring the difference between specimen's weights in air and that soaked in water at room temperature, in which water is used as a floating liquid. The microstructure of composites is studied by both the optical microscope and scanning electron microscopy. Energy-dispersive spectroscopy (SEM/EDS) using a field-emission microscope (FE-SEM). Scanning electron microcopy carried out in Composite Materials Processing lab., JWRI, Osaka University. Also used X-ray diffraction (XRD) technique is applied to identify the phase composition and phase structure of the mixed powders and sintered samples. An advanced diffractometer is used

with Cu K-alpha radiation, operated at 40 kV. X-ray diffraction was carried out in Central Metallurgical R & D Institute (CMRDI) in Cairo, Egypt. The crystallite size was assessed by the classical Williamson-Hall method full width at half maximum (FWHM) from the broadening of XRD peaks and using the following formula [39][40].

$$\frac{\beta cos\theta}{\lambda} = \frac{k}{\mathrm{d}} + 2\varepsilon\left(\frac{2sin\theta}{\lambda}\right) \qquad (1)$$

Where β is the full width at half maximum height (FWHM), θ is the Bragg's angle of the peak, λ is the wavelength of x-ray (0.15406 nm), K is a dimensionless shape factor (0.9), which depends on the material, d is the crystallite size, and ε is the microstrain.

The electrical conductivity, resistivity, and IACS % are estimated, also the thermal conductivity of the sintered samples is along the polished surface of the samples. The test is carried at room temperature. Fig.2 shows the electrical conductivity was carried out in the Faculty of Technology and Education, Suez University.

The measured electrical conductivity is used to estimate the international annealing copper stridulated (IACS %) units according to the standard ASTM: B193-02 Wiedemann and Franz derived a relation between the electrical and thermal conductivity. So, thermal conductivity can be calculated from the measured electrical conductivity using the Wiedemann-Franz law as shown in the following relation [41].

$$\frac{K}{\sigma} = L * T \qquad (2)$$

Where k is the thermal conductivity in W/m.K, σ is the electrical conductivity in (S/m), L is Lorenz's constant number of 2.44 x 10-8 W.Ω/K2, and T is the absolute temperature in °K.

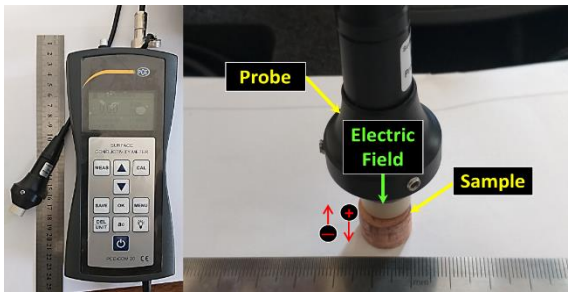

Figure 2 Electrical conductivity measuring device setup.

The abrasive wear rate was carried out by the pin-on-disc method under normal loads of 5, 15, and 25 N according to the standard ASTM: G133-05 [42][43]. Circular specimens with a contact area of 30.1 mm² are loaded on a steel disc that rotates at 132 RPM and a hardness of 64 HRC and surface roughness of 6 µm. The abrasive wear rate of the pins during sliding was described as the weight loss per unit sliding time. The weight loss was measured using an electronic balance with a resolution of 0.0001 g. The tester continuously registered the stationary pin specimen's coefficient of friction and vertical linear displacement. Before each weight calculation, the pins were washed in acetone and dried.

The wear rate is determined according to the following equation [42][43]:

where, ΔW = (W_1 - W_2) = Weight loss (g), W_1 and W_2 are the weights before and after testing, respectively, and T is the sliding time (Sec) = 600 sec.

The hardness was performed using the Shimadzu a Vickers hardness tester (HMV-2T) with a test load of 100 g and a dwell time of 15 s according to ASTM standard E 92. The measurements were taken at twelve different positions for each specimen.

Results and Discussion

Investigation of Cu - TiC and Al_2O_3 Powders

XRD Investigation of Used Powders

Fig.23 shows the XRD patterns of as-received pure Cu, TiC, and Al_2O_3 powders. Only peaks corresponding to Cu, TiC, and Al_2O_3 with high intensities appeared, indicating raw materials purity. Diffraction patterns relative to Cu powder exhibit peaks at 43.24, 50.34, and 74.04°, while those of TiC powder appear at 35.92°, 41.71°, and 60.44°, and those of Al_2O_3 powder appeared at 19.86°, 25.91°, 31.24°, 31.53°, 33.09°, 35.45°, 37.02°, 38.06°, 39.16°, 40.09°, 43.62°, 45.15°, 47.95°, 50.95°, 52.83° and 57.74° without other constituents. The revealed characteristic peaks in the XRD pattern were consistent with JCPDS file JCPDS Card No.04-0836 and JCPDS Card No. 32-1383 and JCPDS Card No. 46-1212 for Cu, TiC, and Al_2O_3, respectively.

Microstructure of Cu, TiC and Al_2O_3

FE-SEM images for as received Cu, TiC, and Al_2O_3 powders are shown in Fig.4 (a), (b) and (c), respectively. Copper has a flake structure with an irregular shape, TiC Particles are fine irregular spherical particles, and Al_2O_3 has also irregular spheres.

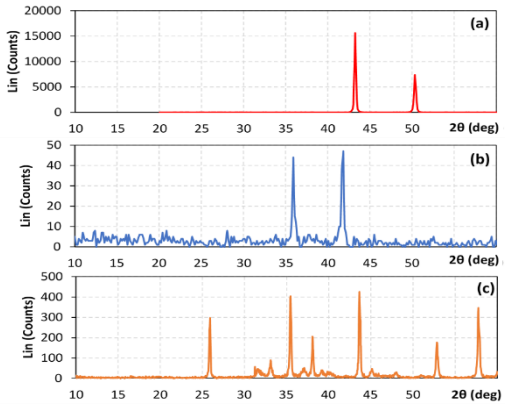

Figure 3 XRD patterns of as-received (a) Cu powder, (b) TiC powder, and (c) Al2O3 powder.

Composite Characterization

XRD patterns of composites after SPS process

Fig. 5 (a) shows the diffraction patterns of the Cu sample which is the blank one. It refers that no peaks rather than those corresponding to the mean peaks of crystallite Cu. This indicates the high purity and crystallinity of the raw

material. Fig. 5 (b) and (c) refers to the XRD of Cu-TiC and Cu- Al_2O_3 composites, respectively. Both indicate the appearance of only Cu and TiC peaks for the Cu-TiC samples and Cu with Al_2O_3 peaks for the Cu- Al_2O_3 composite. This indicates that no new phases are formed between Cu with either TiC or Al_2O_3. Also, no carbide or oxide phases are formed during the sintering process. For fig.5 (d) only three types of peaks have appeared when are corresponding to Cu, TiC, and Al_2O_3. This may be due to the rapid solidification and sintering process by SPS.

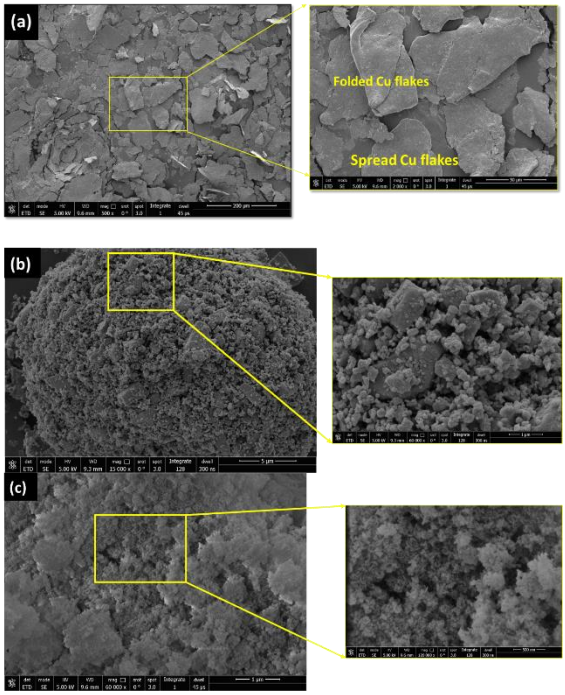

Figure 4 FE-SEM images of; (a) Cu powder, (b) TiC powder, and (c) Al2O3 powder

Fig.6 validates the crystallite size of the reinforced Cu and the SPS composites calculated from X-ray peak broadening. The crystallite size has greatly reduced with the addition of TiC/ Al_2O_3 ceramic particles. In the case of the Cu-Al_2O_3 composite, the crystallite size has decreased by 88%. This decrease in the crystallite size is the main reason for broadening and reducing the peak density due to embedding reinforcements which induce local stress/strain concentration in the copper matrix as well as increasing the work hardening of the copper particles [44][45].

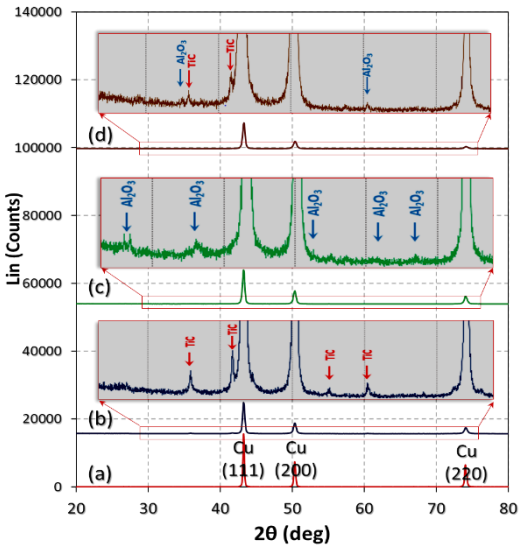

Figure 5 XRD patterns of composites after SPS process. (a) Cu Pure, (b) Cu - 3% wt. TiC, (c) Cu - 3% wt. Al2O3, and (d) Cu/ 1.5% wt. TiC-1.5% wt. Al2O3.

Microstructure Investigation of Composites

Fig.7 shows SEM micrographs of pure Cu, Cu-3wt. %TiC, Cu-3wt. % Al_2O_3, and Cu-3wt. %TiC / Al_2O_3 hybrid nanocomposites, respectively. Fig.7 (b) shows that TiC particles are white spots in the grey copper matrix area, and the distribution of TiC particles is uniform all over the Cu matrix. Also, nano Al_2O_3 particles are distributed uniformly through the Cu matrix, which appears as a black spot. While in Fig.7 (d) higher interconnection between nano TiC and Al_2O_3 particles are observed, also, some agglomerations take place, where it is difficult to distinguish between TiC and Al_2O_3 particles. Also, both TiC and Al_2O_3 nanoparticles are concentrated in the grain boundaries of the Cu matrix and distributed homogeneously. For nearly all samples, very small pores are observed which indicates good densification. The SPS technique is a quick sintering process so no big chance for the formation of any undesirable phases, or any grain growth.

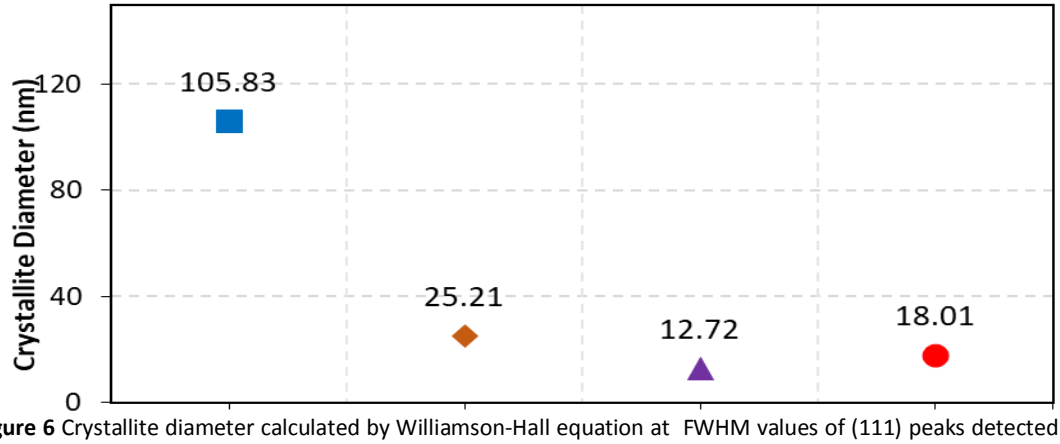

Figure 6 Crystallite diameter calculated by Williamson-Hall equation at FWHM values of (111) peaks detected by XRD.

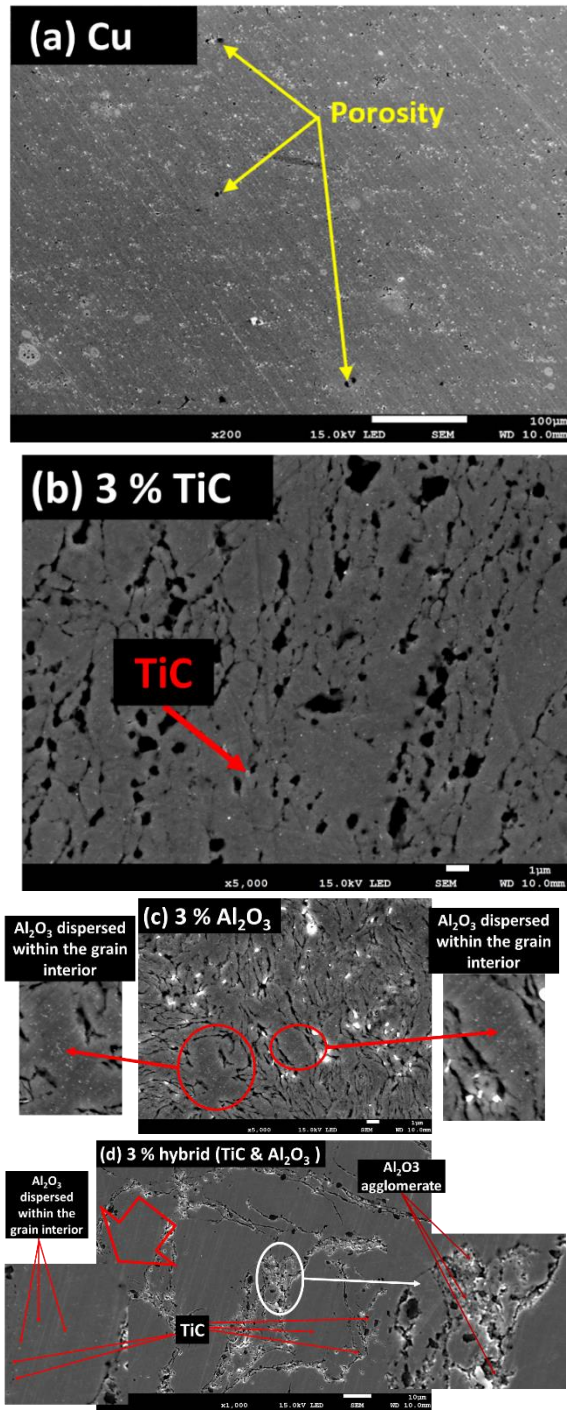

Figure 7 FE-SEM image for (a) S00 (b) S01, (c) S02, and (d) S03; samples.

Density Measurement

The powder pressing and compaction is a very important parameter in the PM technique, in which the density of composite material is the most important parameter which affects greatly physical and mechanical properties. The theoretical density of 3wt. % TiC or Al_2O_3, and 3 % hybrid of TiC / Al_2O_3 mixed with copper powder samples is 8.94, 8.73, 8.61, and 8.67 g/cm^3, respectively. Fig.8 shows that the bulk and relative density of sintered samples decrease with the addition of ceramic reinforcement, while the apparent porosity of sintered samples increases remarkably.

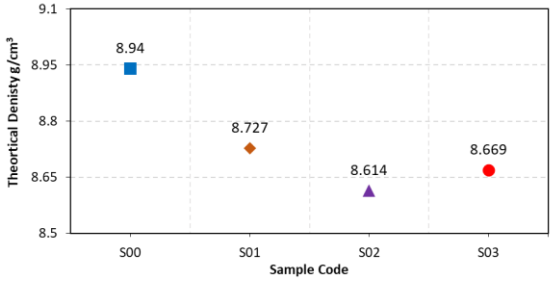

Figure 8 Theoretical density of pure Cu and the prepared composites.

The relative density of the sintered samples is determined using Archimedes' principle as given in Fig.9. Is decreased by adding the ceramic particles in which the relative density of pure Cu "S00", and the nanocomposites "S01", "S02" and "S03" are determined as 97, 94, 95, and 94%, respectively. The large difference between the melting point of Cu metal and the nanoceramics reduces the bonding of the composite's constituents and increases the porosity [46]. The porosity of pure Cu "S00" and the nanocomposites "S01", "S02", and "S03" are, observed at the interface as indicated in Fig.7 (b), (c), and (d). This may be due to the non-wettability problem between copper and ceramic additives. In which large surface energy is produced at the interface between the particles causing some agglomerations and pores [47]. Also, decreasing the density of "S01", "S02" and "S03" samples lower than that of Cu pure may be attributed to the lower density of both TiC and Al_2O_3 than that of Cu 8.94 g/cm^3. The presence of hard-ceramic particles between the ductile Cu particles hinders the densification, so the density decreases.

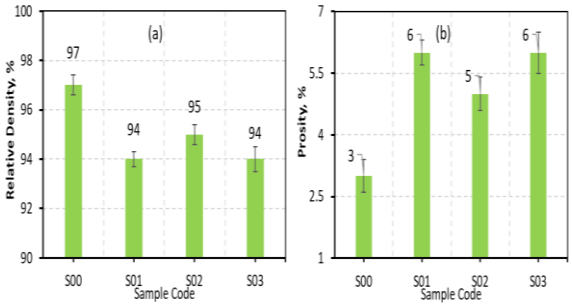

Figure 8 (a) Relative density, and (b) Porosity of pure Cu and sintered composites.

Electrical Conductivity Measurement

The electrical conductivity of pure Cu "S00", and the nanocomposites "S01", "S02", "S03" are determined by PCE-COM 20 electric resistivity instrument. Fig.10 shows the relation between the type of nano-ceramic material additions and the electrical conductivity values. The figure indicates that it decreases with adding the strengthening TiC and Al_2O_3 nanoparticles to the copper matrix. The electrical conductivity of a metal is dependent mainly on the movement of the internal electrons. In situ formation of ceramic reinforcement, nanoparticles can increase the scattering surfaces of electrons in the matrix and reduce the electrical conductivity of the copper matrix composites. The electrical conductivity values of polished samples are given in Table-2 and Fig.10. The addition of ceramics such as titanium carbide or alumina to copper increases its electrical resistivity and decreases the electrical conductivity [1]. The increase of lattice defects

reduces the electron's mean free path and affects the electrical conductivity values [48]. This also can be explained by the zero electrical conductivity values of both TiC and Al_2O_3 which decreases the overall conductivity of the prepared composites [1]. Besides, the non-wettability problem between the metallic Cu and the ceramic TiC and Al_2O_3 causes the formation of pores which decreases the conductivity as the pore conductivity is zero [49].

Table 2 Electrical and thermal conductivity after SPS

No.	Materials after sintering by SPS	Electrical Conductivity (σ) MS/m	Thermal conductivity (K) W/m.k	% IACS	(R) Ω.mm²/m
1	Pure copper	37.5	269.19	64.66	0.02638
2	Cu-3 wt.% TiC	20.76	149.03	35.79	0.04817
3	Cu-3 wt.% Al_2O_3	24.41	175.23	42.09	0.04076
4	Cu-1.5 wt.% TiC & 1.5 wt.% Al_2O_3	20.87	149.82	35.98	0.04778

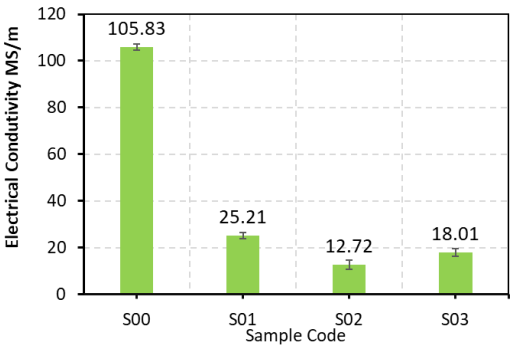

Figure 10 Electrical conductivity of pure Cu and sintered composites.

Thermal Conductivity Estimation

The electrical conductivity of all specimens is measured using a conductivity tester for metals PCE-COM 20. Then, the specific electrical resistivity is determined and converted to international annealed copper standard conductivity (IACS) unit according to ASTM B193. The thermal conductivity is then calculated using Wiedemann–Franz law [41].

Fig.11 and Table 2 shows that the thermal conductivity of pure copper is 269.19 W/m.K. The calculated thermal conductivity of Cu-3wt. % TiC, Cu-3wt. % Al_2O_3, and Cu-3 wt. % TiC/ Al_2O_3 hybrid nanocomposites are 149.03, 175.23, and 149.82 W/m.K, respectively. The decrease in thermal conductivity of nanocomposites by the addition of reinforcement ceramic particles is because the thermal conductivity of used reinforcements is much lower than that of copper. Moreover, agglomeration of some reinforcement particles at grain boundaries increases the scattering of charge carriers and reduces the thermal conductivity. Besides, higher porosity reduces thermal conductivity. Due to the ceramic nature of the added reinforcement materials TiC and Al_2O_3 there is no wettability between either of them with Cu metal. This increases the surface energy between them, so some aggregations take place causing the formation of pores that have zero conductivity consequently the thermal conductivity decreases [35]. There is another observation from the figure is the increase of thermal conductivity value of Cu- Al_2O_3 composite more than the other one. This may be due to the lower porosity of these samples than the other ones.

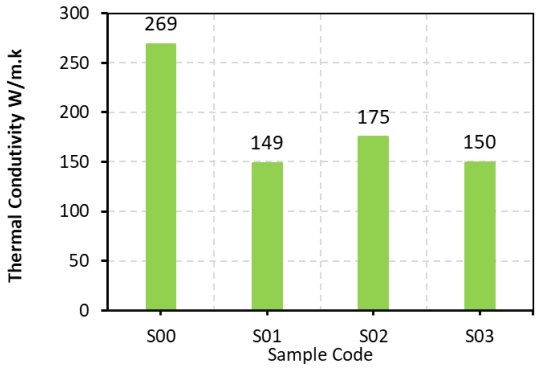

Figure 11 Thermal conductivity of pure Cu and sintered composites.

Tribological properties

The effect of the addition of individual/combine addition of TiC and Al_2O_3 on the abrasive wear is an investigation using variable loads. From Fig.12(a) It can be observed that there are two phenomena, the first is the increase of the wear rate by increasing the applied load for all samples. The effect of load on the surface of the sample is like the scratching, in which as the applied load increases, the depth of the penetration of the indenter increases. The second phenomenon is the high wear resistance for the Cu-TiC sample, followed by Cu- Al_2O_3, while Cu/ (TiC- Al_2O_3) hybrid composite has the highest wear rate compared with that of pure Cu. This may be explained by the addition of a hard ceramic material such as TiC or Al_2O_3 to Cu enhances the wear resistance [19][46]. In which TiC and Al_2O_3 resist the wear due to their high strength that retards the penetration of the load indenters, consequently Cu-TiC and Cu-Al_2O_3 samples have a slower wear rate than pure Cu. Also, the addition of nano TiC or Al_2O_3 to the Cu matrix facilitates the filling of TiC or Al_2O_3 nanoparticles in the interstitial spaces between the Cu particles, so good densification, and a harder surface take place, consequently, the wear resistance is increased, and weight loss was decreased. But hybrid additions of both TiC with Al_2O_3 to Cu matrix increases the wear rate. This may be attributed to the lower density and higher porosity of these samples as the percent of agglomeration takes place due to increasing the surface energy between the two ceramic materials with each other's and with Cu matrix. On the other hand, as shown in Fig.12(b) the hardness results indicated that the incorporation of nanoparticles of TiC and Al_2O_3 significantly improved the mechanical properties of the unreinforced Cu. The hardness of the composites, Cu-3 wt. % TiC, Cu-3 wt. % Al_2O_3, and Cu-1.5wt.%TiC-1.5 wt.% Al_2O_3 composites were 111.9, 149, and 112 VH higher than that of monolithic Cu (81.4 VH), respectively. Thus, increasing the hardness by the addition of hard ceramic TiC or Al_2O_3 particles may be ascribed to the hard nature of the added ceramic materials and the nanoparticles that are distributed all over the Cu matrix. It can also be seen that the Cu reinforced with nano Al_2O_3 particles has a higher hardness than that reinforced with TiC even though the

TiC has a higher hardness than Al_2O_3. This is attributed to two main factors. The first is that the particle size of Al_2O_3 is less than that of TiC by about 50 % since Al_2O_3 has ~50 nm particle size, while TiC has 100 nm. Therefore, the incorporation of finer particles in the nanoscale inside a ductile metal such as Cu enhances the hardness according to the Hall-Petch equation [50]. The second reason is the larger volume fraction of the nano Al_2O_3 than TiC which is widely distributed all over the Cu matrix. This gives the prepared Cu-3 wt. % Al_2O_3 composite more strength and, therefore the hardness increased.

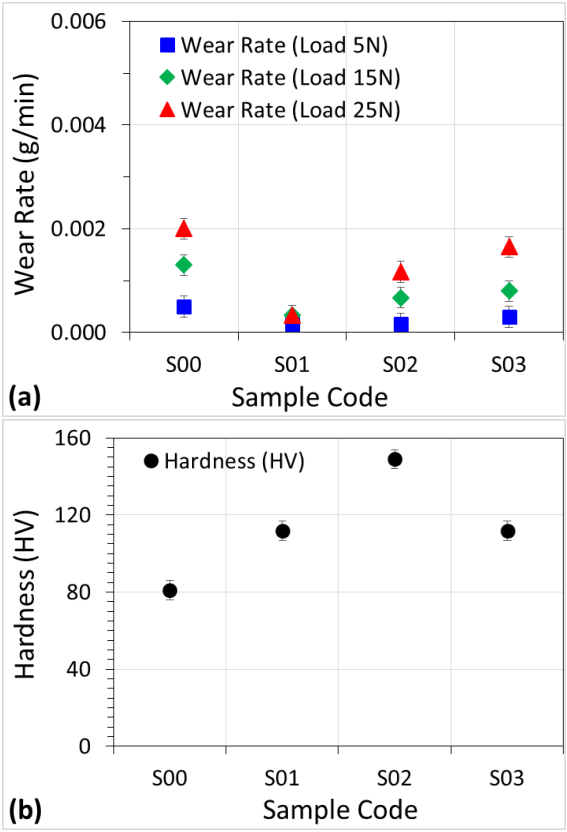

Figure 12 Wear rate and Vickers hardness of Cu pure and sintered composites.

Fig.13 shows that the coefficient of friction significantly was improved with 3 % wt. TiC, also decreased with increased load from 5 to 25 N, while increased with a lesser degree by adding 3 % wt. TiC/ Al_2O_3 into Cu matrix. It is clear from the figure that Cu-TiC and Cu- Al_2O_3 samples have the lowest COF which is compatible with the wear rate results. While Cu-TiC/ Al_2O_3 has the highest COF. This is Due to the highest porosity of this sample, in which the presence of pores facilitates the friction of the surface.

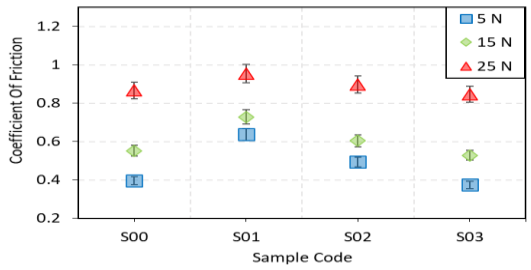

Figure 13 Coefficient of Friction of pure Cu and sintered composites.

CONCLUSION

Powder metallurgy technique is applied to fabricate Cu metal matrix composites reinforced with different nano-ceramic 3wt. %TiC, 3wt. % Al_2O_3 and 3wt. % TiC and Al_2O_3 hybrid nanocomposites.

Based on the present results it could be concluded that:

1. SPS is a successful sintering route for the preparation of Cu-TiC, Cu-Al_2O_3, and Cu/TiC-Al_2O_3 composites since the relative density reach 95 % for sintered copper and 96 % for Cu-TiC sintered composite.

2. The microstructure evaluation reveals a homogeneous distribution of reinforcement for Cu-TiC and Cu-Al_2O_3 and some agglomerations in the hybrid sample Cu/TiC-Al_2O_3 are observed.

3. Addition of 3 wt.% of TiC and Al_2O_3 nanoparticles neither individually nor combined to copper slightly decreases both the electrical and thermal conductivity of Cu-composite.

4. Reinforcing Cu with TiC or Al_2O_3 nanoparticles decreases the wear rate and Coefficient of friction.

5. additions of Al_2O_3 and/or TiC to Cu increase the measured hardness and Cu-3wt. % Al_2O_3 nanocomposites exhibit a higher hardness (149 HV).

ABBREVIATIONS

Cu Copper

TiC Titanium Carbide

Al_2O_3 Alumina

SPS Spark Plasma Sintering

HSPS Hybrid Spark Plasma Sintering

BPR Ball to Powder Ratio

PCA Process Controlling Agent

XRD X-ray Diffraction

FWHM Full Width at Half Maximum

JCPDS Joint Committee on Powder Diffraction Standards

FE-SEM Field Emission Scanning Electron Microscope

COF Coefficient of Friction

IACS International Annealed Copper Standard Conductivity

Acknowledgement

The authors acknowledge the kind support by Prof. Katsuyoshi Kondoh, Composite Materials Processing lab., JWRI, Osaka University, for providing the spark plasma sintering machine in his lab to do the consolidation of the composites and thank the researchers and the technicians of the Central Metallurgical R & D Institute (CMRDI) in Cairo, Egypt for their collaboration.

Recommendations

We are highly recommended in future work the using of the different percentage above and below 3 wt. % of TiC and Al_2O_3.

Data availability: The data that support the findings of this study are included in the article. Any further requested information can be addressed to the corresponding author.

Conflicts of Interest: The authors declared no potential conflicts of interest concerning the research, authorship, and/or publication of this article.

Conflict of Interest

No conflict to declare

REFERENCES

[1] S. V Wankhede, "Modelling of Cu-Al_2O_3 Metal Matrix Composite Prepared By Powder Metallurgy Route," *Int. J. Eng. Adv. Technol.*, no. 3, pp. 2249–8958, 2013, [Online]. Available: http://citeseerx.ist.psu.edu/viewdoc/download?doi=10.1.1.687.5144&rep=rep1&type=pdf.

[2] F. Akhtar, S. J. Askari, K. A. Shah, X. Du, and S. Guo, "Microstructure, mechanical properties, electrical conductivity and wear behavior of high volume TiC reinforced Cu-matrix composites," *Mater. Charact.*, vol. 60, no. 4, pp. 327–336, 2009, doi: 10.1016/j.matchar.2008.09.014.

[3] N. T. H. Oanh, N. H. Viet, J. S. Kim, and D. V. Dudina, "Structural investigations of TiC–Cu nanocomposites prepared by ball milling and spark plasma sintering," *Metals (Basel).*, vol. 7, no. 4, pp. 9–11, 2017, doi: 10.3390/met7040123.

[4] W. Zhai, W. Lu, Y. Chen, X. Liu, L. Zhou, and D. Lin, "Gas-atomized copper-based particles encapsulated in graphene oxide for high wear-resistant composites," *Compos. Part B Eng.*, vol. 157, no. July 2018, pp. 131–139, 2019, doi: 10.1016/j.compositesb.2018.08.125.

[5] Y. Liu, Z. Yang, B. Tian, Y. Zhang, Z. Gu, and A. A. Volinsky, "Hot Deformation Behavior of the 20 vol.% TiC/Cu-Al_2O_3 Composites," *J. Mater. Eng. Perform.*, vol. 27, no. 9, pp. 4791–4798, 2018, doi: 10.1007/s11665-018-3586-1.

[6] X. Wang *et al.*, "Phase composition and magnetic properties of Pr–Nd–MM–Fe–B nanocrystalline magnets prepared by spark plasma sintering," *Rare Met.*, vol. 39, no. 1, pp. 36–40, 2020, doi: 10.1007/s12598-019-01265-8.

[7] X. H. Zhang, C. G. Lin, S. Cui, and Z. De Li, "Microstructure and properties of Al_2O_3 dispersion-strengthened copper fabricated by reactive synthesis process," *Rare Met.*, vol. 33, no. 2, pp. 191–195, 2014, doi: 10.1007/s12598-013-0149-3.

[8] M. A. Lagos, I. Agote, G. Atxaga, O. Adarraga, and L. Pambaguian, "Fabrication and characterisation of Titanium Matrix Composites obtained using a combination of Self propagating High temperature Synthesis and Spark Plasma Sintering," *Mater. Sci. Eng. A*, vol. 655, pp. 44–49, 2016, doi: 10.1016/j.msea.2015.12.050.

[9] M. R. Akbarpour and S. Alipour, "Wear and friction properties of spark plasma sintered SiC/Cu nanocomposites," *Ceram. Int.*, vol. 43, no. 16, pp. 13364–13370, 2017, doi: 10.1016/j.ceramint.2017.07.037.

[10] D. L. Yung, S. Cygan, M. Antonov, L. Jaworska, and I. Hussainova, "Ultra high-pressure spark plasma sintered ZrC-Mo and ZrC-TiC composites," *Int. J. Refract. Met. Hard Mater.*, vol. 61, pp. 201–206, 2016, doi: 10.1016/j.ijrmhm.2016.09.014.

[11] L. Vinet and A. Zhedanov, "A 'missing' family of classical orthogonal polynomials," *Acta Univ. Agric. Silvic. Mendelianae Brun.*, vol. 53, no. 9, pp. 1689–1699, Nov. 2010, doi: 10.1088/1751-8113/44/8/085201.

[12] M. A. Volosova, A. A. Okunkova, S. V. Fedorov, K. Hamdy, and M. A. Mikhailova, "Electrical Discharge Machining Non-Conductive Ceramics: Combination of Materials," *Technologies*, vol. 8, no. 2, p. 32, 2020, doi: 10.3390/technologies8020032.

[13] A. Knaislová, P. Novák, S. Cygan, L. Jaworska, and M. Cabibbo, "High-pressure spark plasma sintering (HP SPS): A promising and reliable method for preparing Ti-Al-Si alloys," *Materials (Basel).*, vol. 10, no. 5, pp. 6–13, 2017, doi: 10.3390/ma10050465.

[14] A. Elsayed, "W-Cu- CNT Nanocomposite by Vacuum Sintering and Hot Isostatic Pressing," *Nanosci. Nanotechnol.*, vol. 6, pp. 35–38, 2016, doi: 10.5923/c.nn.201601.0 6.

[15] S. Z. Zhu, D. L. Gong, Z. Fang, and Q. Xu, "Preparation and properties of ZrB2-Cu composites by spark plasma sintering," *Key Eng. Mater.*, vol. 512–515, pp. 739–743, 2012, doi: 10.4028/www.scientific.net/KEM.512-515.739.

[16] T. Peng, Q. Yan, X. Zhang, and Y. Zhuang, "Role of titanium carbide and alumina on the friction increment for Cu-based metallic brake pads under different initial braking speeds," *Friction*, Nov. 2020, doi: 10.1007/s40544-020-0439-3.

[17] L. Li, Y. S. Wong, J. Y. H. Fuh, and L. Lu, "EDM performance of TiC/copper-based sintered electrodes," *Mater. Des.*, vol. 22, no. 8, pp. 669–678, Dec. 2001, doi: 10.1016/S0261-3069(01)00010-3.

[18] H. M. Yehia, F. Nouh, and O. El-Kady, "Effect of graphene nano-sheets content and sintering time on the microstructure, coefficient of thermal expansion, and mechanical properties of (Cu /WC –TiC-Co) nano-composites," *J. Alloys Compd.*, vol. 764, pp. 36–43, 2018, doi: 10.1016/j.jallcom.2018.06.040.

[19] A. M. Sadoun, M. M. Mohammed, A. Fathy, and O. A. El-Kady, "Effect of Al2O3 addition on hardness and wear behavior of Cu-Al_2O_3 electro-less coated Ag

nanocomposite," *J. Mater. Res. Technol.*, vol. 9, no. 3, pp. 5024–5033, 2020, doi: 10.1016/j.jmrt.2020.03.020.

[20] M. R. Akbarpour, H. Mousa Mirabad, M. Khalili Azar, K. Kakaei, and H. S. Kim, "Synergistic role of carbon nanotube and SiCn reinforcements on mechanical properties and corrosion behavior of Cu-based nanocomposite developed by flake powder metallurgy and spark plasma sintering process," *Mater. Sci. Eng. A*, vol. 786, p. 139395, Jun. 2020, doi: 10.1016/j.msea.2020.139395.

[21] Y. Pan *et al.*, "Microstructure and tribological properties of titanium matrix composites reinforced with in situ synthesized TiC particles," *Mater. Charact.*, vol. 170, p. 110633, Dec. 2020, doi: 10.1016/j.matchar.2020.110633.

[22] A. M. Sadoun, M. M. Mohammed, E. M. Elsayed, A. F. Meselhy, and O. A. El-Kady, "Effect of nano Al_2O_3 coated Ag addition on the corrosion resistance and electrochemical behavior of Cu-Al_2O_3 nanocomposites," *J. Mater. Res. Technol.*, vol. 9, no. 3, pp. 4485–4493, 2020, doi: 10.1016/j.jmrt.2020.02.076.

[23] A. Abu-Oqail, A. Wagih, A. Fathy, O. Elkady, and A. M. Kabeel, "Effect of high energy ball milling on strengthening of Cu-ZrO2 nanocomposites," *Ceram. Int.*, vol. 45, no. 5, pp. 5866–5875, 2019, doi: 10.1016/j.ceramint.2018.12.053.

[24] H. Asgharzadeh and S. Eslami, "Effect of reduced graphene oxide nanoplatelets content on the mechanical and electrical properties of copper matrix composite," *J. Alloys Compd.*, vol. 806, pp. 553–565, Oct. 2019, doi: 10.1016/j.jallcom.2019.07.183.

[25] R. Zheng, N. Li, and Z. Zhan, "Friction and wear behavior of Cu-La_2O_3 composite sliding against 52100 bearing steel in vacuum," *Vacuum*, vol. 161. pp. 55–62, 2019, doi: 10.1016/j.vacuum.2018.12.019.

[26] X. Fan, X. Huang, Q. Liu, H. Ding, H. Wang, and C. Hao, "The microstructures and properties of in-situ ZrB_2 reinforced Cu matrix composites," *Results Phys.*, vol. 14, no. May, p. 102494, 2019, doi: 10.1016/j.rinp.2019.102494.

[27] D. Ning, A. Zhang, and H. Wu, "Enhanced Wear Performance of Cu-Carbon Nanotubes Composite Coatings Prepared by Jet Electrodeposition," *Materials (Basel).*, vol. 12, no. 3, p. 392, Jan. 2019, doi: 10.3390/ma12030392.

[28] Q. Zhao, X. Gan, and K. Zhou, "Enhanced properties of carbon nanotube-graphite hybrid-reinforced Cu matrix composites via optimization of the preparation technology and interface structure," *Powder Technol.*, vol. 355, pp. 408–416, Oct. 2019, doi: 10.1016/j.powtec.2019.07.055.

[29] E. Geethendra Kumar, M. Ahasan, K. Venkatesh, and K. S. B. S. V. S. Sastry, "Design, fabrication of Powder Compaction Die and Sintered behavior of Copper Matrix Hybrid Composite," *International Research Journal of Engineering and Technology*. 2018, [Online]. Available: www.irjet.net.

[30] A. Miranda-López, C. A. León-Patiño, E. A. Aguilar-Reyes, E. Bedolla-Becerril, and G. Rodriguez-Ortiz, "Effect of graphite addition on wear behaviour of hybrid Cu/TiC-Gr infiltrated composites," *Wear*, p. 203793, Mar. 2021, doi: 10.1016/j.wear.2021.203793.

[31] H. Mostaan, M. Z. Mehrizi, M. Rafiei, R. Beygi, and A. R. Abbasian, "Contribution of mechanical activation and annealing in the formation of nanopowders of Al(Cu)/TiC-Al2O3 hybrid nanocomposite," *Ceram. Int.*, vol. 43, no. 2, pp. 2680–2685, Feb. 2017, doi: 10.1016/j.ceramint.2016.11.082.

[32] R. G. Chandrakanth, K. Rajkumar, and S. Aravindan, "Fabrication of copper–TiC–graphite hybrid metal matrix composites through microwave processing," *Int. J. Adv. Manuf. Technol.*, vol. 48, no. 5–8, pp. 645–653, May 2010, doi: 10.1007/s00170-009-2474-0.

[33] R. G. Chandrakanth, K. Rajkumar, and S. Aravindan, "Fabrication of copper-TiC-graphite hybrid metal matrix composites through microwave processing," *Int. J. Adv. Manuf. Technol.*, vol. 48, no. 5–8, pp. 645–653, 2010, doi: 10.1007/s00170-009-2474-0.

[34] A. Abu-Oqail, A. Samir, A. R. S. Essa, A. Wagih, and A. Fathy, "Effect of GNPs coated Ag on microstructure and mechanical properties of Cu-Fe dual-matrix nanocomposite," *Journal of Alloys and Compounds*, vol. 781. pp. 64–74, 2019, doi: 10.1016/j.jallcom.2018.12.042.

[35] M. Venkateswarlu, M. Ashok Kumar, and K. Hema Chandra Reddy, "Thermal Behavior of Spark Plasma Sintered Ceramic Matrix-Based Nanocomposites," *J. Bio-Tribo-Corrosion*, vol. 6, no. 2, pp. 6013–6028, 2020, doi: 10.1007/s40735-020-00355-w.

[36] Q. Zhao, X. Gan, and K. Zhou, "Enhanced properties of carbon nanotube-graphite hybrid-reinforced Cu matrix composites via optimization of the preparation technology and interface structure," *Powder Technol.*, vol. 355, pp. 408–416, 2019, doi: 10.1016/j.powtec.2019.07.055.

[37] O. O. Ayodele, M. B. Shongwe, P. A. Olubambi, B. A. Obadele, and T. Langa, "Hybrid Spark Plasma Sintering of Materials: A Review," *Int. J. Mater. Mech. Manuf.*, vol. 6, no. 6, pp. 360–364, 2018, doi: 10.18178/ijmmm.2018.6.6.407.

[38] A. Fathy, O. Elkady, and A. Abu-Oqail, "Production and properties of Cu-ZrO_2 nanocomposites," *J. Compos. Mater.*, vol. 52, no. 11, pp. 1519–1529, 2018, doi: 10.1177/0021998317726148.

[39] M. R. Akbarpour, H. Mousa Mirabad, M. Khalili Azar, K. Kakaei, and H. S. Kim, "Synergistic role of carbon nanotube and SiCn reinforcements on mechanical properties and corrosion behavior of Cu-based nanocomposite developed by flake powder metallurgy and spark plasma sintering process," *Mater. Sci. Eng. A*, vol. 786, no. April, p. 139395, 2020, doi: 10.1016/j.msea.2020.139395.

[40] M. R. Akbarpour, H. Mousa Mirabad, S. Alipour, and H. S. Kim, "Enhanced tensile properties and electrical conductivity of Cu-CNT nanocomposites processed via the

combination of flake powder metallurgy and high pressure torsion methods," *Mater. Sci. Eng. A*, vol. 773, no. September 2019, p. 138888, 2020, doi: 10.1016/j.msea.2019.138888.

[41] H. Yi *et al.*, "Wiedemann-Franz law of Cu-coated carbon fiber," *Carbon N. Y.*, vol. 162, pp. 339–345, 2020, doi: 10.1016/j.carbon.2020.02.062.

[42] M. R. Akbarpour, M. Najafi, S. Alipour, and H. S. Kim, "Hardness, wear and friction characteristics of nanostructured Cu-SiC nanocomposites fabricated by powder metallurgy route," *Mater. Today Commun.*, vol. 18, pp. 25–31, Mar. 2019, doi: 10.1016/j.mtcomm.2018.11.001.

[43] H. Nautiyal, P. Srivastava, O. P. Khatri, S. Mohan, and R. Tyagi, "Wear and friction behavior of copper based nano hybrid composites fabricated by spark plasma sintering," *Mater. Res. Express*, vol. 6, no. 8, 2019, doi: 10.1088/2053-1591/ab28a2.

[44] K. K. Alaneme and B. U. Odoni, "Mechanical properties, wear and corrosion behavior of copper matrix composites reinforced with steel machining chips," *Eng. Sci. Technol. an Int. J.*, vol. 19, no. 3, pp. 1593–1599, Sep. 2016, doi: 10.1016/j.jestch.2016.04.006.

[45] M. R. Akbarpour, E. Salahi, F. Alikhani Hesari, A. Simchi, and H. S. Kim, "Fabrication, characterization and mechanical properties of hybrid composites of copper using the nanoparticulates of SiC and carbon nanotubes," *Mater. Sci. Eng. A*, vol. 572, pp. 83–90, Jun. 2013, doi: 10.1016/j.msea.2013.02.039.

[46] I. FARÍAS, L. OLMOS, O. JIMÉNEZ, M. FLORES, A. BRAEM, and J. VLEUGELS, "Wear modes in open porosity titanium matrix composites with TiC addition processed by spark plasma sintering," *Trans. Nonferrous Met. Soc. China (English Ed.*, vol. 29, no. 8, pp. 1653–1664, 2019, doi: 10.1016/S1003-6326(19)65072-7.

[47] W. M. Daoush and O. A. Elkady, "Microstructure, physical properties and hardness of alumina short fibres/nickel matrix composites fabricated by powder technology," *J. Compos. Mater.*, vol. 48, no. 30, pp. 3735–3746, 2014, doi: 10.1177/0021998313513203.

[48] J. Mirazimi, P. Abachi, and K. Purazrang, "Spark plasma sintering of ultrafine YSZ reinforced Cu matrix functionally graded composite," *Acta Metall. Sin. (English Lett.*, vol. 29, no. 12, pp. 1169–1176, 2016, doi: 10.1007/s40195-016-0512-0.

[49] Z. Q. Yang, Y. Liu, B. H. Tian, and Y. Zhang, "Hot compression performance of TiC10/Cu-AL2O3 composite prepared by vacuum hot-pressed sintering," *Adv. Mater. Res.*, vol. 750–752, pp. 99–102, 2013, doi: 10.4028/www.scientific.net/AMR.750-752.99.

[50] H. Deng, J. Yi, C. Xia, and Y. Yi, "Mechanical properties and microstructure characterization of well-dispersed carbon nanotubes reinforced copper matrix composites," *J. Alloys Compd.*, vol. 727, pp. 260–268, 2017, doi: 10.1016/j.jallcom.2017.08.131.